Title: Effects of Self-Assembling Monolayer Modification of NiOx Nanoparticles Layer on the Performance of Inverted Perovskite Solar Cells and Application in High Power-Per-Weight Devices

Authors: Qin Wang, Ph.D; Chu-Chen Chueh; Ting Zhao; Morteza Eslamian; Wallace C.H. Choy; Alex K.-Y. Jen

To be cited as: 10.1002/cssc.201701262

Link to VoR: https://doi.org/10.1002/cssc.201701262

Effects of Self-Assembling Monolayer Modification of NiO_x Nanoparticles Layer on the Performance of Inverted Perovskite Solar Cells and Application in High Power-Per-Weight Devices

Qin Wang[a,c], Chu-Chen Chueh[a], Ting Zhao[a], Jiaqi Cheng[d], Morteza Eslamian*[c], Wallace C.H. Choy[d] and Alex K.-Y. Jen*[a,b]

Abstract: Entirely low-temperature solution-processed (≤ 100 °C) planar p-i-n perovskite solar cells (PVSCs) offer great potential for commercialization of roll-to-roll fabricated photovoltaic devices. However, the stable inorganic hole transporting layer (HTL) in PVSCs is usually processed at high temperature (200 °C ~500 °C) which is far beyond the tolerant temperature (≤ 150 °C) of roll-to-roll fabrication. In this context, inorganic NiO_x nanoparticles (NPs) are an excellent candidate to serve as the HTL in PVSCs, owing to their excellent solution-processability at room temperature. However, the low-temperature processing condition is usually accompanied with defect formation, which deteriorates the film quality and device efficiency, to a large extent. To suppress this setback, we used a series of benzoic acid self-assembly monolayers (SAMs) to passivate the surface defects of the NiO_x NPs, and found that 4-bromobenzoic acid could effectively play the role of the surface passivation. This SAM layer reduces the trap-assisted recombination, minimizes the energy offset between the NiO_x NPs and perovskite, and changes the HTL surface wettability, thus enhances the perovskite crystallization, resulting in more stable PVSCs with enhanced power conversion efficiency (PCE) of 18.4%, exceeding the control device PCE (15.5%). Also, we incorporated the above-mentioned SAMs into flexible PVSCs (F-PVSCs) and achieved one of the highest PCE of 16.2% on polyethylene terephthalate (PET) substrate with a remarkable power-per-weight of 26.9 W/g. This facile interfacial engineering method offers great potential for the large-scale manufacturing and commercialization of PVSCs.

The intriguing perovskite solar cells (PVSCs) have aroused tremendous interest, due to their excellent optoelectronic properties, long charge carrier lifetime, low-temperature solution processability, and relatively low fabrication cost, with a remarkable certified power conversion efficiency (PCE) of 22.1%, which could now compete with the commercialized silicon solar cells, if the device stability can be improved.[1] Generally speaking, the current state-of-the-art PVSCs adopt a planar heterojunction architecture that could be fabricated with either n-i-p or p-i-n structure, due to the ambipolar transport property of the perovskite light harvesters.[2] However, the n-i-p type suffers from severe hysteresis setback due to the unbalanced charge distribution in the perovskite layer.[3] Considering the fact that the electron diffusion length in perovskite is relatively longer than the hole diffusion length, the p-i-n structure is more advantageous to obtain a reasonably stable device performance.[4, 5] Employing a suitable hole transporting layer (HTL) is a prerequisite for developing a high performance p-i-n PVSC, because the HTL not only facilitates effective hole collection, it also minimizes the interfacial charge recombination.[6]

The most frequently-used HTL in PVSCs is poly(3,4-ethylenedioxythiophene): polystyrene sulfonate (PEDOT:PSS) and nickel oxide (NiO_x). Although PEDOT: PSS is a commercialized and standard HTL material, it suffers from several intrinsic problems such as hygroscopicity, acidity-induced instability, and large potential loss due to unmatched energy level with the adjacent layers in the PVSC structure.[7] In contrast, p-type NiO_x is advantageous due to its large band gap (3.5-3.9 eV)[8], deep valence band (5.1 eV-5.4 eV),[9-11] high mobility (~10^{-3} $cm^2V^{-1}s^{-1}$),[12, 13] induced by the large doping of Ni^{3+} ion[13], and its superior stability,[14] resulting from its inorganic nature, which brings about a longer device lifetime.[15] To date, a variety of processing strategies for the fabrication of NiO_x thin films have been reported, such as sol-gel,[16] sputtering,[12] pulsed laser deposition,[10] spray pyrolysis,[14] electrochemical deposition[17] and so on. However, most of the current techniques either require high temperature deposition processes or high temperature post treatment, which are not compatible with the roll-to-roll fabrication.[18] Recently, room temperature solution-processed NiO_x nanoparticles (NPs)[8, 11, 19-21, 22, 23] have been considered as the building blocks for NiO_x thin films. Choy et al. employed non-stoichiometric NiO_x NPs with a cubic rock-salt structure and octahedral Ni^{2+} and O^{2-} sites as the HTL in organic and perovskite solar cells.[11, 19, 20] These room temperature solution-processed NPs based NiO_x films (in the following context, we use NiO_x to refer to all the NPs based NiO_x) demonstrated excellent optoelectronic properties, without the need for post-treatment. By changing the preparation method, Yin et al. deposited low-temperature solution-processed NiO_x films on flexible poly(ethylene 2,6-naphthalate) (PEN) substrates and fabricated flexible PVSC with a PCE of 13.43%.[22] Hou et al. adopted low-temperature solution-processed NiO_x nanocrystal ink to fabricate PVSCs with PCE of 17.5% and achieved a potential loss as low as 0.226 V.[23] Although the PCE of p-i-n

[a] Q. Wang, Dr. C.C. Chueh, T. Zhao, Prof. A.K.Y. Jen
Department of Materials Science and Engineering
University of Washington
Seattle, WA, 98105, USA
E-mail: ajen@uw.edu
[b] Prof. A.K.Y Jen
Department of Materials Science & Engineering
City University of Hong Kong
Kowloon, Hong Kong, SAR China
[c] Prof. M. Eslamian
University of Michigan–Shanghai Jiao Tong University Joint Institute
Shanghai, 200240, China
Email: Morteza.Eslamian@sjtu.edu.cn
[d] J. Cheng, Prof. W.C.H. Choy,
Department of Electrical and Electronic Engineering
The University of Hong Kong
Pokfulam, Hong Kong, SAR China

Supporting information for this article is given via a link at the end of the document.

type PVSCs incorporating NiO_x HTL has surpassed 17%, it is still barely satisfactory compared with the n-i-p type PVSCs, due mainly to their inferior fill factor (FF) and current density.[4] This may be ascribed to the fact that the low-temperature processing of metal oxides usually leaves behind defects in the film structure. Such defects, therefore, result in poor contact between the NiO_x film and the perovskite layer, which not only influences the perovskite crystallinity and morphology, but also causes charge recombination and lower light absorption.[9, 10, 24]

One potential approach to simultaneously tackle the morphology and charge selectivity problems is to use self-assembled monolayers (SAMs),[25-27] which has been proved as an effective way to change the interfacial properties between a charge transfer layer (CTL) and the perovskite layer.[6, 28] Typically, SAMs are thermodynamically-favored ordered monolayer-forming modifiers comprising a head group, a spacer, and a tail group. The head group could be anchored to the surface through physisorption or a preferred chemisorption. The spacer group determines separation of the intermolecular interactions, which is usually in the form of aromatic rings or alkane chains.[26] The tail group could be designed to endow various functions via synthetic chemistry, where such functional groups could in turn remarkably alter the wettability of the upper layer, fascinating the deposition of the forthcoming layer through both dipolar and dispersive interactions,[29] where this further influences the crystallinity, morphology and energy level offset.[25, 30, 31] Recently, Snaith and Jen et al. reported a C_{60}-SAM deposited on titanium dioxide (TiO_2) that had electronic coupling with the perovskite layer and achieved a significantly reduced device hysteresis.[32] Han et al. applied an organic silane SAM to the TiO_2-perovskite interface in order to change the crystallinity and morphology of the perovskite, and achieved efficient fully-printable PVSCs. Zuo et al. adopted C_3-SAM[33] and 4-pyridinecarboxylic acid SAM[34] to tailor the energy levels of zinc oxide and tin dioxide thin films, respectively, and observed significant enhancement in the photovoltaic performance. However, most of current works in the PVSCs field that have used SAMs to modify the interfacial properties between the CTL and perovskite layer are centered about the electron transfer layer (ETL) in n-i-p type PVSCs. The application of SAMs to modify the HTL has few example, especially for low-temperature solution-processed NiO_x HTL in p-i-n type PVSCs.

In this work, we first systematically investigated the separate role of the chemical interaction between the NP-based NiO_x and perovskite layers by inserting suitable parasubstituted benzoic acid (R-BA) SAMs, as depicted in Scheme 1. According to Choy et al.,[11, 20] the surface functional groups of the NiO_x NPs are the hydroxylated group which can react with the carboxyl groups[9, 35] The purpose of using the SAMs with different dipole moments are as follows: (1) to serves as a “glue” to improve the adhesion between the NiO_x films and the ionic perovskite layer in order to better facilitate the charge transfer by passivating inorganic surface trap states;[34, 36] (2) to modify the work function (WF) of the NiO_x NPs through their molecular ordering induced by the permanent dipole moments;[27] (3) to change the perovskite crystallinity and morphology via chemical interactions by means of different terminated functional groups.[33, 37] The gas-phase dipole moments of the benzoic acid derivatives are increased in sequence when the tail groups are substituted by $–NH_2$ (-4.5 D)< $–OCH_3$ (-3.9 D)< –H (-2.1 D)[38] < –Cl (2.0 D) < –Br (2.1 D),[27, 34, 39] in which H-BA shows the van der Waals interaction, while others present dipolar interactions.[34] The Br-BA modifier was found to have a positive effect which largely enhanced the PCE to 18.4% with increased open-circuit voltage (V_{oc}) of 1.11 V, short-circuit current density (J_{sc}) of 21.7 mA cm^{-2}, and FF of 76.3%. In addition, the device stability was improved owing to the minimization of the energy level offset, reduced surface trap states, increased perovskite crystallinity, and enhanced wetting between NiO_x and perovskite layers, outperforming the control group (PCE of 15.5%) in terms of both the PCE and stability. Moreover, we incorporated the Br-BA SAM into the flexible PVSCs (F-PVSCs) and achieved one of the highest PCE of 16.2% on the PET substrate with a remarkable power-per-weight (PPW) of 26.9 W/g, This simple and facile surface modification technique may further pave the way for the scaling up of the PVSCs through roll-to-roll manufacturing processes.

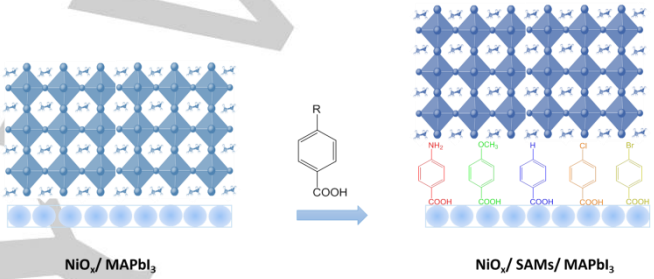

Scheme 1. Schematic diagram of the NiO_x/ $MAPbI_3$ structure (left) and NiO_x/ SAMs/ $MAPbI_3$ structure

The fabrication of SAM modified NiO_x films can be briefly described as follows: NiO_x NPs solution was first spun onto ITO glass and then different SAMs were spun onto the NiO_x films. After a short while low-temperature annealing, we used ethanol to wash the film surface to remove the remaining SAMs. Scanning electron microscopy (SEM) was used to investigate the effect of depositing R-BA on the morphology of NiO_x. As is shown in Figure S1, the surface morphology of pristine NiO_x films and SAMs treated NiO_x films did not change much, all showing good coverage with some pinhole-like black dots area. Figure S2 showed that Br-BA has reacted with the hydroxylated functional group of NiO_x through the Fourier-transform infrared spectroscopy.

Then we explored the morphology evolution and grain size distribution of methylammonium iodide ($MAPbI_3$) perovskite layer deposited atop different R-BA modified NiO_x films in Figure 1a and Figure 1b. By inserting different SAMs with different terminated functional group, the perovskite morphology and grain size all varies to a large extent. For example, the average perovskite grain size (AGZ) of the Ref group is 140 nm and its morphology shows some pinholes while for the NH_2-BA modified NiO_x films, larger pinholes are present and the AGZ increases to 203 nm. In particular, the Br-BA modified film surprisingly shows pinhole-free film with an AGZ of 287 nm, which is more than double that of the Ref group. This great enhancement can be ascribed to the terminated functional group of Br may change the

surface wetting of NiO_x films, thus contributes to the larger perovskite grain size.[31] Moreover, it may also interact with the MA^+ ions to improve the adhesion through hydrogen bonding, which is another reason for the smooth and flawless perovskite film, confirming by enlarged SEM images shown in the Figure S3.[28]

The crystallinity of the $MAPbI_3$ perovskite films made on different R-BA modified underlayers was investigated by X-ray diffraction (XRD), as shown in Figure S4, where the characteristic peaks at 13.9°, 28.3° and 31.8° correspond to the (110), (220), and (310) crystal planes, respectively. The perovskite based on the Br-BA SAM has the most intensive peak in the (110) plane, which manifests the enhanced crystallinity compared with the Ref group. The full width at half maximum (FWHM) peaks associated with the (110) plane, illustrated in Figure 1c, are a more vivid way to further elucidate the dislocation or vacancies in the $MAPbI_3$ perovskite films, made on various underlayers.[40] The corresponding FWHM values of the Ref and NH_2-BA based perovskites show the same value of 0.184, which may be ascribed to the pinhole formation as shown in Figure 1a. Then it reaches a lowest value of 0.137 for the Br-BA based perovskite. The decreased value indicates decreased vacancies and proves the enhanced crystallinity, which is consistent with the bottom morphology images of Figure 1a.

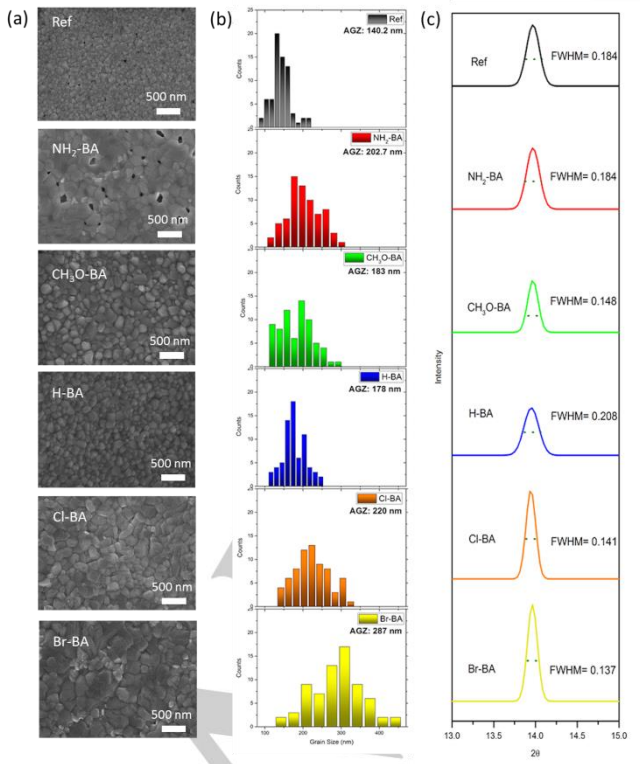

Figure 1. The morphology of (a) the perovskite film deposited on various R-BA modified NiO_x films; (b) grain size distribution of perovskite on various R-BA modified NiO_x films; (c) Gaussian distribution of the peak of the (110) plane and the FWHM value of perovskite film on the R-BA modified NiO_x layer..

The WF of R-BA modified NiO_x NPs films were characterized by the ultraviolet photoelectron spectroscopy (UPS). As is shown in Figure 2a, the WF of Ref is 5.21 eV. If we use SAMs with negative dipole moment, say NH_2-BA, CH_3O-BA and H-BA, to modify the surface of NiO_x NPs, the WF calculated from the secondary cutoff will decrease to 4.82 eV, 4.96 eV and 5.06 eV, respectively. However, for the NiO_x NPs films modified by Cl-BA and Br-BA whose dipole moment is positive, the WF respectively increases to 5.36 eV and 5.4 eV which is aligned with the valence band maximum of $MAPbI_3$. This implies that SAM with positive dipole moment can increase the WF of NiO_x NPs films.

To investigate the effect of the R-BA modification on the device performance, we fabricated PVSCs based on the following device structure, also shown in Figure S5: ITO/NiO_x (with or without SAM)/$MAPbI_3$/PCBM/bis-C_{60}/Ag, where PCBM is the short form for [6,6]-phenyl-C_{61}-butyric acid methylester. As shown in Figure S6 and Table S1 of the Supporting Information, the PCE of the PVSCs based on the pristine NiO_x film is 15.5% with a high V_{oc} of 1.07 V, which is similar to those obtained in the previous work.[20] The NH_2-BA and CH_3O-BA modified devices show worse PECs, while the H-BA, Cl-BA and Br-BA modification is found to enhance the device efficiency. The NH_2-BA modified device has the worst PCE, presumably due to a large density of pinholes (see Figure 1a) in the associated perovskite layer. In contrast, the Br-BA modified device shows the highest PCE of 18.4%, with photovoltaic parameters enhanced compared with those of the Ref device, e.g., the V_{oc} increased from 1.07 to 1.11 V, J_{sc} increased from 19.6 to 21.7 mA cm^{-2}, and FF increased from 74.2 to 76.3%. This enhancement echoes the positive effect of the modification of NiO_x film by Br-BA (c.f. the bottom images of Figure 1a and 1b), which has led to the formation of pinhole-free, well-covered, and highly crystalline perovskite with suitable energy level alignment. The enhanced UV-Visible absorption of the Br-BA modified perovskite in Figure S7 also corroborates the improvement of J_{sc}.

We found that the V_{oc} decreases if a SAM modifier with negative dipole moment is applied, whereas the V_{oc} increases if the dipole moment is positive, which is well correlated with the WF change (ΔWF) of SAM modified NiO_x films. To investigate this observation, the variations of the V_{oc} and ΔWF versus the dipole moment are shown in Figure 2b. Remarkably, the V_{oc} and ΔWF correlates well with the dipole magnitude through a linear relationship, which implies that the energy level offset between the NiO_x and perovskite could be fine-tuned by the virtue of the dipole moments,[41] although the surface dipole concentration and the tilt angle between the dipole and the substrate may also have certain influences.[39] In fact, the dipole could induce a step in the vacuum level under the effect of an electrical field. As illustrated in Figure 2c, the unmodified NiO_x has an energy level offset with the valence band maximum of the $MAPbI_3$ perovskite. After the interface modification by SAMs, the WF and the band edge will be changed and affect the V_{oc}, which is ideally determined by the effective band gap between the WF of NiO_x and the quasi-Fermi level of the conduction band in the $MAPbI_3$ perovskite. Additionally, if the surface dipole is pointed away from the NiO_x, the band edge will shift upward and the effective gap will reduce, i.e. the V_{oc} decreases. However, if the surface dipole is pointed towards the NiO_x, the band edge will shift downward, increasing the effective gap and consequently the V_{oc} will

increase. Our results are consistent with this band bending theory.

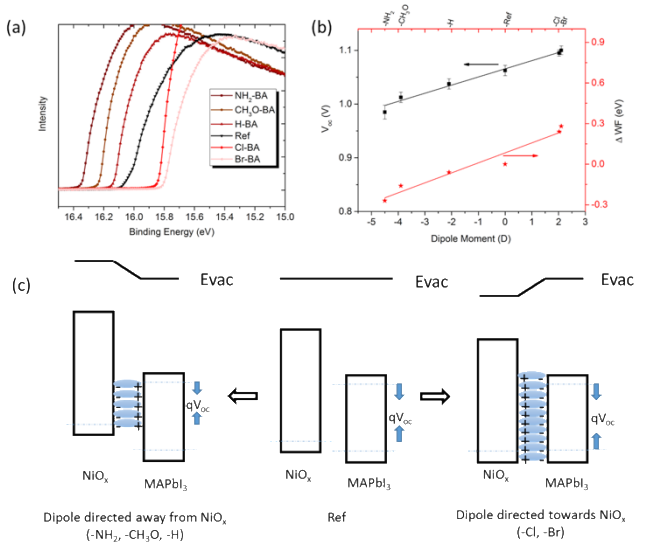

Figure 2. (a) UPS curves of PVSCs without or with various SAM modifications; (b) V_{oc} and Δ WF plotted against the dipole moment of the SAMs; (c) schematic diagram of the band bending, caused by the SAMs with different dipole moments. Quasi-Fermi levels are shown as dashed lines.

In order to further investigate the merit of the SAMs modification, in Figure 3a and Table 1, we have respectively shown the *J-V* curves and the photovoltaic parameters of the best-performing Ref and the Br-BA modified PVSCs under both forward and reverse scan directions with a voltage sweeping rate of 0.1 V s^{-1}. For the Ref device, there is subtle but obvious hysteresis resulting in PCE of 15.3% under the forward scan, and slightly different PCE of 15.5% under the reverse scan. However, the Br-BA modification eliminates the hysteresis, showing a constant PCE value of 18.4%, regardless of the scan direction. We further examined the scan rates of 0.01, 0.05, and 0.5 V s^{-1}, and found that the PCEs of the Br-BA modified devices show negligible hysteresis, which further corroborates the reliability of the Br-BA modification (c.f. Figure S8). The enhanced J_{sc} of the Br-BA modified PVSC may be attributed to the increased absorption and crystallinity of the perovskite layer, which is also confirmed by the corresponding external quantum efficiency (EQE) spectrum shown in Figure 3b. The improved FF value of the Br-BA modified devices (c.f. Table 1) is speculated to be due to effective pinhole passivation on the NiO_x NPs surfaces (c.f. Figure 2a) and the enhanced interfacial hole extraction,[42] resulting in an improved contact between the NiO_x and perovskite layers via the SAM linkages.

The steady state output power has been proved as a more precise way to quantify the true PCE of solar cells.[43] By applying a bias around the maximum output power (0.89 V for the Ref device, and 0.93 V for the Br-BA based device), under AM 1.5 G and one sun condition, the steady state PCE of the studied devices were recorded as 14.6 and 17.8%, respectively, as shown in Figure 3c, which clearly verifies the device performance enhancement by the Br-BA modification. The histograms of the PCE of 32 fabricated devices with and without Br-BA modification are shown in Figure 3d. It is observed that the average PCE of the Ref devices shows a PCE of 14.5%, while that of the Br-BA modified devices leaps to 17% with a normal distribution, substantiating decent reproducibility and reliability of the modification technique.

The device stability or the long-term lifetime is another crucial photovoltaic parameter, since it determines its suitability for commercialization.[44] We therefore traced the PCE of the Ref and Br-BA modified devices under the humidity of around 30% for 15 days, as shown in Figure 3e. The Ref device maintained 70% of its original PCE, whereas the Br-BA modified device maintained about 80% of its original PCE. The enhancement may be attributed to the enhanced crystallinity of the perovskite layer and decreased defect states of the NiO_x film, where the former improves the stability of the perovskite lattice, and the latter impedes the permeation of water and oxygen into the inner perovskite film.[45]

We also compared the PCE versus processing temperature made by other groups that focus on the application of the NiO_x in PVSCs (Figure 3f and Table S2). Although a newly accepted work about cesium doped NiO_x based PVSCs achieved a record efficiency of more than 19%, its high temperature process (275 °C) severely restricted its application in flexible device fabrication,[46] In terms of a viewpoint of commericialization, all the layers should be processed under 150 °C. Based on the Figure 3f, our work substantiates the importance of the employed low-temperature processed Br-BA modified NiO_x films incorporated in the PVSCs.

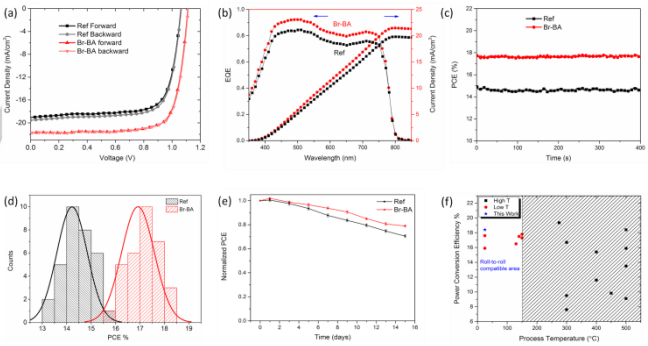

Figure 3. (a) J-V curves of the Ref and the Br-BA modified PVSCs under forward and reverse scan, at the scan rate of 0.1 V s^{-1}; (b) EQE spectrum and the cumulative J_{sc} of the Br-BA modified champion device; (c) steady state output power of the PVSCs with and without Br-BA modification; (d) PCE distribution of the devices with and without Br-BA modification; (e) stability of the PVSCs with and without Br-BA modification over 15 days stored under humidity of ~30%; (f) PCE versus process temperature of the PVSCs incorporating NiO_x layer, made in this work and by others in similar works. The data about other group's work and its corresponding reference can be found in Table S2.

Table 1. Photovoltaic parameters of Ref and Br-BA based PVSCs.

Sample	V_{oc} (V)	J_{sc} (mA cm^{-2})	FF %	PCE %
Ref forward	1.07	19.1	74.8	15.3
Ref backward	1.07	19.6	74.2	15.5
Br-BA forward	1.11	21.7	76.3	18.4
Br-BA backward	1.11	21.7	76.3	18.4

In order to better understand and ascertain the influence of the Br-BA SAMs on the NiO_x film defects and perovskite crystallization, we obtained the photoluminescence (PL) spectra (Figure 4a and 4b), to examine the photocarrier dynamics of the $MAPbI_3$ perovskite deposited atop the NiO_x film.[47, 48] The steady state PL intensity of $MAPbI_3$ deposited atop the NiO_x film is significantly lower than that deposited on bare glass, indicating that NiO_x could effectively transfer the charges. As we deposited the Br-BA SAM between the NiO_x and $MAPbI_3$ layers, the PL intensity is further reduced, suggesting its role in surface passivation of the NiO_x film, in which the charge carrier could be more effectively transferred in the device. This phenomenon can also explain the enhanced J_{sc} in the Br-BA modified PVSCs. The time resolved PL (TRPL) decay of the studied devices are shown in Figure 4b, where the TRPL curves demonstrate an obvious bi-exponential decay behavior. The fast decay portion of the spectrum corresponds to the trap states quenching or charge transfer, while the longer decay portion reflects the bi-molecular recombination.[34, 47] Compared with the $MAPbI_3$ on the bare glass, the NiO_x could effectively quench the PL due to its hole transporting ability. It is observed that the PL quenching of the Br-BA modified NiO_x film is further enhanced. The Br-BA modification not only helps the formation of a more uniform crystalline perovskite film, which is an indicative of shorter PL lifetime compared with the perovskite formed on the pristine NiO_x film, but also functions as the linking agent between the NiO_x and perovskite layers. Based on the data shown in Figure 4b, we believe that the better contact induced by the Br-BA SAMs contributes to electrical coupling in the interfacial layer, and therefore results in an improved J_{sc}, as discussed before.

To understand the recombination mechanism of the studied devices, the *J-V* curves of the pristine and Br-BA modified devices were obtained under light intensities ranging from 1 to 100 mW cm^{-2}, as shown in Figure S9. The power law dependence of the J_{sc} on the light intensity ($J \sim I^{\alpha}$) is plotted in Figure 4c. According to the previous reports, α will be equal to 0.75, if the device has a space charge limit due to the imbalanced carriers, or it will be equal to 1, if there is no space charge effects.[49] In this work, for the pristine devices, α equals 0.88, whereas for the Br-BA modified devices it equals 0.91, indicating that the Br-BA modified device is less affected by the space charge limit. This suggests that the Br-BA modification could reduce the charge recombination and potential barriers, which could be envisaged to be a result of defect passivation on the NiO_x surface.[50]

Since all photo-generated carriers will finally recombine in the open circuit condition, investigating the relationship between the V_{oc} and light intensity is a cogent method to precisely probe the trap-assisted recombination mechanism. By plotting the natural logarithmic relation between the V_{oc} and the light intensity in Figure 4d, we calculated the slope of the Ref and Br-BA modified devices, which are equal to 1.7kT/q and 1.5kT/q, respectively, where k is the Boltzmann constant, q is the electron charge, and T is the temperature in Kelvins. It has been reported that a trap-free relationship would have a slope of 1kT/q, while for the Shockley-Read-Hall recombination, the slope would be 2kT/q.[51] Therefore, it is deduced that the Br-BA modified devices have less trap-assisted recombination compared with the Ref devices. Combined with the morphology diagrams in Figure 1a and 1b, we found that this reduced recombination results from the surface passivation of the NiO_x films and better crystallization of the perovskite layer, which collectively enhance the device photovoltaic performance

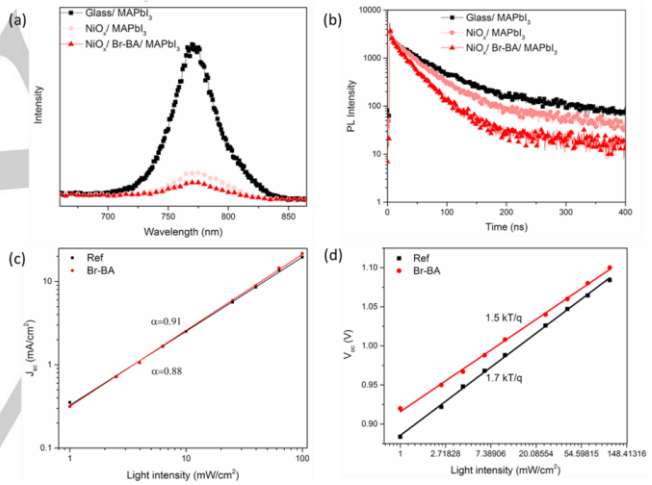

Figure 4. (a) Steady state PL, and (b) TRPL of the perovskite films made on bare glass, NiO_x, and Br-BA modified NiO_x films; light intensity dependence of (c) the J_{sc}, and (d) V_{oc} of the studied devices with and without Br-BA modification.

As another major task, we then exploited the Br-BA SAM modification method on flexible PVSCs devices (F-PVSCs). The J-V curves depicted in Figure 5a show the photovoltaic performance of the champion devices of the Br-BA modified PVSC made on glass and the F-PVSC made on the flexible PET substrate. As a major consequence, the FF drops significantly from 76.3% on glass to 71.3% on PET, and the J_{sc} decreases to 20.7 mA cm^{-2}, but the V_{oc} maintains its value (1.10 V for PET versus 1.11 V for glass). This trend is reasonable since the flexible PET substrate might deteriorate an effective contact between each layer and thus induces the low FF and J_{sc}.[20, 22, 52] Even though the F-PVSCs show a relatively lower PCE compared with the devices made on glass, the PCE of the Br-BA modified F-PVSCs reaches 16.2%, which is one of the highest PCE values for the F-PVSCs, demonstrating the merit of the

Br-BA SAM modification technique. For the reliability measurements, we have analyzed the PCE histogram of the F-PVSCs over 32 devices in Figure 5b and the average value is around 15%, substantiating its decent reproducibility. In order to investigate the flexibility influence on the device performance, we have conducted the mechanical bending test as shown in Figure 5c. The F-PVSCs could retain 75% of its initial PCE even after 110 bending cycles, proving the decent mechanical stability. The inset picture in Figure 5c shows the flexibility of the fabricated F-PVSCs.

We have also summarized the recent works about NiO_x HTL based F-PVSCs whose PCEs are larger than 10% (see Table S3) and compared the PCE and V_{oc} values with this work in Figure 5d. It is observed that the F-PVSC in this work shows the highest performance compared with other NiO_x based F-PVSC. In addition, the V_{oc} of the Br-BA modified F-PVSCs of this work is significantly higher than those reported by the others, which could be ascribed to the better interface between the NiO_x and the perovskite layers, owing to the insertion of the Br-BA SAM modifier.

An important figure of merit of the optoelectronic devices is their power-per-weight (PPW) ratio, since it could combine and demonstrate the overall outcome of the high PCE, flexibility, and light weight. Figure 5e compares the typical PPW of the conventional crystalline silicon and inorganic and organic thin film solar cells, where it is found that the F-PVSC made in this work outperforms all other solar cells and achieves a remarkable PPW of 26.9 W/g (see Table S4).[53] Figure 5f is the F-PVSC made in this work placed on a green leaf, substiating its light weight

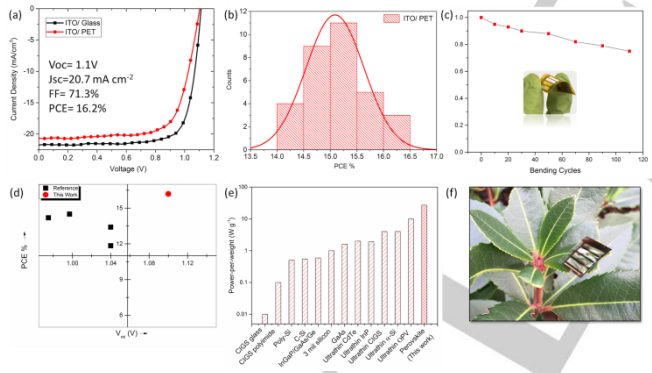

Figure 5. (a) J-V curves of the Br-BA modified PVSCs made on glass substrates and F-PVSCs made on flexible PET substrate; (b) PCE distribution of the Br-BA modified F-PVSCs over 32 devices; (c) normalized PCE of the Br-BA modified F-PVSCs, as a function of the bending cycles and the inset image is the photograph of the F-PVSC; (d) comparison of the PCE and V_{oc} of the NiO_x based F-PVSCs in this work and by others; (e) power-per-weight (PPW) comparison of various photovoltaic technologies (cell data are extracted from Reference [52]); (f) photograph of the fabricated ultralight SAM modified F-PVSC placed on a leaf.

In conclusion, we have developed a benzoic acid derivative SAM interfacial modification method applied on low-temperature processed NiO_x HTL based inverted PVSCs. By using a series of SAMs with different dipole moments, we found that the SAM with positive dipole moments induces a band bending downward in the interface of the NiO_x NPs and the perovskite layer, which could minimize the energy level offsets between the aforementioned layers, and consequently enhance the device V_{oc}. The best device performance was obtained through the Br-BA SAM modification by which the surface defects of the NiO_x NPs were passivated and enhanced the perovskite crystallization. The collective positive effects of the SAM modification, including better energy level alignment, better interfacial contact, surface passivation, and enhanced crystallization boosted the PCE of the studied devices to 18.4%, with V_{oc} of 1.11 V, J_{sc} of 21.7 mA cm^{-2}, and FF of 76.3%, as well as enhanced stability, outperforming the reference device with an inferior PCE of 15.5% and lower stability. Also we applied the same SAM modification method on F-PVSC and achieved one of the highest PCE of 16.2% with a remarkable power-per-weight of 26.9 W/g. Our research shed light on the concept of the interfacial engineering applied to low-temperature solution-processed metal oxide HTLs used in p-i-n PVSCs, and the device performance results corroborated the great potential and promise of this technique for the development of commercially-viable rigid or flexible PVSCs.

Experimental Section

Materials: Methylammonium iodide (MAI) and bis-C_{60} were home-made according to the procedure outlined in a previous work.[54] The NP-based NiO_x thin films were synthesized according to the literature.[20] Other materials were purchased and used, as received.

Solution preparation: NiO_x NPs with a size distribution of about 5~10 nm were dispersed in water (20 mg ml^{-1}), and then ultrasonicated for 8 hours; 180 mg of MAI and 555 mg of lead iodide were dissolved in 1 ml of a mixture of dimethyl sulfoxide (DMSO) and gamma-butyrolactone (GBL) solution (volume ratio of 3:7, respectively), and the resulting solution was stirred overnight. R-BA was dissolved in ethanol (2 mg ml^{-1}), and PCBM powder was dissolved in chloroform (CF) (15 mg ml^{-1}). Bis-C_{60} was dispersed in isopropanol (IPA) and ultrasonicated for 3 hours. All solutions were filtered before use.

Perovskite fabrication: ITO-coated glasses were first washed by detergent, deionized water, acetone, and IPA. Each washing process took 10 min. Then ITO-coated glasses were treated in an UV-O_3 furnace for 15 minutes to increase the surface energy and make the ITO surface more hydrophilic. For the flexible devices, the PET substrate was used, as received. Then the dispersion of NiO_x NPs in water was spun onto the ITO-coated glass or PET substrates at 3000 rpm, for 30 s. R-BA solution was spun onto the NiO_x film at 2000 rpm, for 30 s. The monolayer of the molecules was formed either through physical or chemical bonding between the R-BA and NiO_x NPs. The film was annealing on a hotplate at 90° for 5 min. In order to remove the physically-absorbed molecules, ethanol was spun onto the film at 2000 rpm for 30 s for several times. The R-BA modified films were immediately transferred into a glovebox.Then the perovskite solution was spun onto the SAM layer in two steps: first the solution was spun at 1000 rpm for 15 s, and then the speed was immediately increased to 4000 rpm and spinning continued for another 45 s. During the last 25 s, 800 µl of toluene was dropped onto the spinning film in a continuous manner. Then the substrate was placed on a hotplate at 100 °C, for 10 min. After the sample was cooled to the room temperature, the PCBM solution was spun over at 4000 rpm, for 30 s, and then the bis-C_{60} solution was spun at 3000 rpm, for another 30 s. Finally, 120 nm of silver was thermally evaporated under high vacuum (< 1 × 10^{-6}

Torr) to complete the device. The device area was measured with a nonfractive mask with apenture of 0.1 cm^2 to define the illumination area.

Characterization: The morphology of NiO_x and perovskite films was examined by an FEI Sirion XL30 SEM. The XRD data of the perovskite films were obtained using a Bruker F8 Focus Powder XRD machine. The UV-Vis absorption spectra of the perovskite films were recorded by a Varian Cary 5000 spectrophotometer. The UPS was carried out under a discharged lamp with energy of 21.2 eV. The steady-state PL spectra were measured according to our previous study.[7] To obtain the TRPL spectra of the perovskite films with and without Br-BA modification, the films made on bare glass were first encapsulated by poly(methyl methacrylate) (PMMA), and then were placed under 510 nm laser head (LDH-P-C-510, PicoQuant, GmbH) pulsed at a repetition rate of 1 MHz, with a pulse duration of 117 ps. The *J-V* curves were measured using a 450 W xenon lamp solar simulator, using the AM 1.5 G filter, and a Keithley 2400 source meter. A KG3-filtered standard silicon photodiode detector was used to calibrate the light intensity before the measurements. The EQE spectra were obtained using an instrument equipped with a chopper with the frequency of 100 Hz, a Newport Cornerstone 130 monochromator, a standard Research Corp SR830 amplifier, a Keithley 2400 source meter, a silicon photodiode, which is certified by the National Institute of Standards and Technology (NIST) for calibration, and a xenon lamp (Oriel, 300 W). The stability measurements were conducted in a drybox filled with calcium oxide to control and maintain the relative humidity of 30% at room temperature.

Acknowledgements

This work was partially supported by the Office of Naval Research Perovskite Project (N00014-17-1-2260), the Office of Naval Research OPV Project (N00014-17-1-2201) the National Science Foundation (DMR-1608279), the Department of Energy SunShot (DE-EE0006710), and the Asian Office of Aerospace R&D (FA2386-15-1-4106). Q.W. thanks the financial support from the China Scholarship Council (CSC N 201506230080). W. C.H.Choy would like to acknowledge the support of the General Research Fund (Grant 17211916 and 17204117) from the Research Grants Council of Hong Kong Special Administrative Region, China. A.K.-Y.J. is thankful for financial support from the Boeing−Johnson Foundation.

Keywords: self-assembly monolayer (SAM) • flexible perovskite solar cell • energy level alignment • interfacial engineering • band bending

[1] M. A. Green, K. Emery, Y. Hishikawa, W. Warta, E. D. Dunlop, *Prog. Photovolt: Res. Appl.* **2016**, *24*, 905.

[2] J. H. Heo, S. H. Im, J. H. Noh, T. N. Mandal, C.-S. Lim, J. A. Chang, Y. H. Lee, H.-j. Kim, A. Sarkar, M. K. Nazeeruddin, M. Graetzel, S. I. Seok, *Nat. Photonics* **2013**, *7*, 487.

[3] N. J. Jeon, J. H. Noh, W. S. Yang, Y. C. Kim, S. Ryu, J. Seo, S. I. Seok, *Nature* **2015**, *517*, 476; V. W. Bergmann, S. A. Weber, F. J. Ramos, M. K. Nazeeruddin, M. Grätzel, D. Li, A. L. Domanski, I. Lieberwirth, S. Ahmad, R. Berger, *Nat. Commun.* **2014**, *5*, 5001.

[4] W. Yan, S. Ye, Y. Li, W. Sun, H. Rao, Z. Liu, Z. Bian, C. Huang, *Adv. Energy Mater.* **2016**, *6*, 1600474.

[5] Z. Bin, J. Li, L. Wang, L. Duan, *Energy Environ. Sci.* **2016**, *9*, 3424; Y. Wu, X. Yang, W. Chen, Y. Yue, M. Cai, F. Xie, E. Bi, A. Islam, L. Han, *Nat. Energy.* **2016**, *1*, 16148.

[6] C.-C. Chueh, C.-Z. Li, A. K. Y. Jen, *Energy Environ. Sci.* **2015**, *8*, 1160.

[7] Q. Wang, C.-C. Chueh, M. Eslamian, A. K.-Y. Jen, *ACS Appl. Mater. Interfaces* **2016**, *8*, 32068.

[8] J. Kim, H. J. Park, C. P. Grigoropoulos, D. Lee, J. Jang, *Nanoscale* **2016**, *8*, 17608.

[9] Y. Bai, H. Chen, S. Xiao, Q. Xue, T. Zhang, Z. Zhu, Q. Li, C. Hu, Y. Yang, Z. Hu, F. Huang, K. S. Wong, H.-L. Yip, S. Yang, *Adv. Funct. Mater.* **2016**, *26*, 2950.

[10] J. H. Park, J. Seo, S. Park, S. S. Shin, Y. C. Kim, N. J. Jeon, H. W. Shin, T. K. Ahn, J. H. Noh, S. C. Yoon, C. S. Hwang, S. I. Seok, *Adv. Mater.* **2015**, *27*, 4013.

[11] F. Jiang, W. C. Choy, X. Li, D. Zhang, J. Cheng, *Adv. Mater.* **2015**, *27*, 2930.

[12] J. H. Kim, P. W. Liang, S. T. Williams, N. Cho, C. C. Chueh, M. S. Glaz, D. S. Ginger, A. K. Y. Jen, *Adv. Mater.* **2015**, *27*, 695.

[13] S. Liu, R. Liu, Y. Chen, S. Ho, J. H. Kim, F. So, *Chem. Mater.* **2014**, *26*, 4528.

[14] W. Chen, Y. Wu, Y. Yue, J. Liu, W. Zhang, X. Yang, H. Chen, E. Bi, I. Ashraful, M. Gratzel, L. Han, *Science* **2015**, *350*, 944.

[15] S. T. Williams, A. Rajagopal, C. C. Chueh, A. K. Jen, *J. Phys. Chem. Lett.* **2016**, *7*, 811.

[16] Z. Zhu, Y. Bai, T. Zhang, Z. Liu, X. Long, Z. Wei, Z. Wang, L. Zhang, J. Wang, F. Yan, S. Yang, *Angew. Chem. Int. Ed.* **2014**, *53*, 12571; X. Yin, Z. Yao, Q. Luo, X. Dai, Y. Zhou, Y. Zhang, Y. Zhou, S. Luo, J. Li, N. Wang, *ACS Appl. Mater. Interfaces* **2017**, *9*, 2439.

[17] I. J. Park, G. Kang, M. A. Park, J. S. Kim, S. W. Seo, D. H. Kim, K. Zhu, T. Park, J. Y. Kim, *ChemSusChem* **2017**.

[18] F. C. Krebs, *Sol. Energy Mater. Sol. Cells* **2009**, *93*, 394.

[19] H. L. Zhu, J. Cheng, D. Zhang, C. Liang, C. J. Reckmeier, H. Huang, A. L. Rogach, W. C. Choy, *ACS Nano* **2016**, *10*, 6808.

[20] H. Zhang, J. Cheng, F. Lin, H. He, J. Mao, K. S. Wong, A. K. Jen, W. C. Choy, *ACS Nano* **2016**, *10*, 1503.

[21] X. Yin, J. Liu, J. Ma, C. Zhang, P. Chen, M. Que, Y. Yang, W. Que, C. Niu, J. Shao, *J. Power Sources* **2016**, *329*, 398; U. Kwon, B.-G. Kim, D. C. Nguyen, J.-H. Park, N. Y. Ha, S.-J. Kim, S. H. Ko, S. Lee, D. Lee, H. J. Park, *Sci. Rep.* **2016**, *6*, 35994.

[22] X. Yin, P. Chen, M. Que, Y. Xing, W. Que, C. Niu, J. Shao, *ACS Nano* **2016**, *10*, 3630.

[23] Y. Hou, W. Chen, D. Baran, T. Stubhan, N. A. Luechinger, B. Hartmeier, M. Richter, J. Min, S. Chen, C. O. Quiroz, N. Li, H. Zhang, T. Heumueller, G. J. Matt, A. Osvet, K. Forberich, Z. G. Zhang, Y. Li, B. Winter, P. Schweizer, E. Spiecker, C. J. Brabec, *Adv. Mater.* **2016**, *28*, 5112.

[24] W. C. Choy, D. Zhang, *Small* **2016**, *12*, 416.

[25] H. Ma, H. L. Yip, F. Huang, A. K. Y. Jen, *Adv. Funct. Mater.* **2010**, *20*, 1371.

[26] S. A. Paniagua, A. J. Giordano, O. L. Smith, S. Barlow, H. Li, N. R. Armstrong, J. E. Pemberton, J. L. Bredas, D. Ginger, S. R. Marder, *Chem. Rev.* **2016**, *116*, 7117.

[27] H.-L. Yip, S. K. Hau, N. S. Baek, H. Ma, A. K. Y. Jen, *Adv. Mater.* **2008**, *20*, 2376.

[28] X. Li, M. I. Dar, C. Yi, J. Luo, M. Tschumi, S. M. Zakeeruddin, M. K. Nazeeruddin, H. Han, M. Grätzel, *Nature Chem.* **2015**.

[29] P. E. Laibinis, G. M. Whitesides, *J. Am. Chem. Soc.* **1992**, *114*, 1990.

[30] J. Haruyama, K. Sodeyama, L. Han, Y. Tateyama, *J. Phys. Chem. Lett.* **2014**, *5*, 2903.

[31] C. Bi, Q. Wang, Y. Shao, Y. Yuan, Z. Xiao, J. Huang, *Nat. Commun.* **2015**, *6*, 7747.

[32] A. Abrusci, S. D. Stranks, P. Docampo, H. L. Yip, A. K. Jen, H. J. Snaith, *Nano Lett.* **2013**, *13*, 3124.

[33] L. Zuo, Z. Gu, T. Ye, W. Fu, G. Wu, H. Li, H. Chen, *J. Am. Chem. Soc.* **2015**, *137*, 2674.

[34] L. Zuo, Q. Chen, N. De Marco, Y.-T. Hsieh, H. Chen, P. Sun, S.-Y. Chang, H. Zhao, S. Dong, Y. Yang, *Nano Lett.* **2016**.

[35] H. Boehm, *Discuss. Faraday Soc.* **1971**, *52*, 264.

[36] S. K. Hau, H.-L. Yip, O. Acton, N. S. Baek, H. Ma, A. K. Y. Jen, *J. Mater. Chem.* **2008**, *18*, 5113.

[37] L. Liu, A. Mei, T. Liu, P. Jiang, Y. Sheng, L. Zhang, H. Han, *J. Am. Chem. Soc.* **2015**, *137*, 1790.

[38] M. Bruening, E. Moons, D. Cahen, A. Shanzer, *J. Phys. Chem.* **1995**, *99*, 8368.

[39] C. Goh, S. R. Scully, M. D. McGehee, *J. Appl. Phys.* **2007**, *101*, 114503.

[40] N. Li, Z. Zhu, C.-C. Chueh, H. Liu, B. Peng, A. Petrone, X. Li, L. Wang, A. K. Y. Jen, *Adv. Energy Mater.* **2016**, 1601307.

[41] S. Rühle, M. Greenshtein, S.-G. Chen, A. Merson, H. Pizem, C. S. Sukenik, D. Cahen, A. Zaban, *J. Phys. Chem. B* **2005**, *109*, 18907.

[42] S. Chen, S. Yang, H. Sun, L. Zhang, J. Peng, Z. Liang, Z.-S. Wang, *J. Power Sources* **2017**, *353*, 123; M. Cha, P. Da, J. Wang, W. Wang, Z. Chen, F. Xiu, G. Zheng, Z.-S. Wang, *J. Am. Chem. Soc.* **2016**, *138*, 8581.

[43] H. J. Snaith, A. Abate, J. M. Ball, G. E. Eperon, T. Leijtens, N. K. Noel, S. D. Stranks, J. T.-W. Wang, K. Wojciechowski, W. Zhang, *J. Phys. Chem. Lett.* **2014**, *5*, 1511.

[44] G. Niu, X. Guo, L. Wang, *J. Mater. Chem. A* **2015**, *3*, 8970.

[45] J. M. Ball, A. Petrozza, *Nat. Energy*. **2016**, *1*, 16149.

[46] W. Chen, F. Z. Liu, X. Y. Feng, A. B. Djurišić, W. K. Chan, Z. B. He, *Adv. Energy Mater.* **2017**.

[47] Q. Chen, H. Zhou, T. B. Song, S. Luo, Z. Hong, H. S. Duan, L. Dou, Y. Liu, Y. Yang, *Nano Lett.* **2014**, *14*, 4158.

[48] S. D. Stranks, G. E. Eperon, G. Grancini, C. Menelaou, M. J. P. Alcocer, T. Leijtens, L. M. Herz, A. Petrozza, H. J. Snaith, *Science* **2013**, *342*, 341.

[49] V. Mihailetchi, J. Wildeman, P. Blom, *Phys. Rev. Lett.* **2005**, *94*, 126602; L. Koster, V. Mihailetchi, H. Xie, P. Blom, *Appl. Phys. Lett.* **2005**, *87*, 203502.

[50] D. Zhao, M. Sexton, H.-Y. Park, G. Baure, J. C. Nino, F. So, *Adv. Energy Mater.* **2015**, *5*, 1401855.

[51] M. Mandoc, F. Kooistra, J. Hummelen, B. De Boer, P. Blom, *Appl. Phys. Lett.* **2007**, *91*, 263505; R. N. Hall, *Phys. Rev.* **1952**, *87*, 387.

[52] M. Kaltenbrunner, G. Adam, E. D. Głowacki, M. Drack, R. Schwödiauer, L. Leonat, D. H. Apaydin, H. Groiss, M. C. Scharber, M. S. White, *Nat. Mater.* **2015**, *14*, 1032.

[53] H. Zhang, J. Cheng, D. Li, F. Lin, J. Mao, C. Liang, A. K. Y. Jen, M. Grätzel, W. C. Choy, *Adv. Mater.* **2017**.

[54] P. W. Liang, C. Y. Liao, C. C. Chueh, F. Zuo, S. T. Williams, X. K. Xin, J. Lin, A. K. Jen, *Adv. Mater.* **2014**, *26*, 3748; C.-Z. Li, C.-C. Chueh, H.-L. Yip, K. M. O'Malley, W.-C. Chen, A. K. Y. Jen, *J. Mater. Chem.* **2012**, *22*, 8574.

COMMUNICATION

Low-temperature solution-processed NiO_x nanoparticle film is usually accompanied with defect formation. In this work, we find that 4-bromobenzoic acid can form a self-assembled monolayer (SAM) on NiO_x film and effectively tune the interfacial properties, resulting in perovskite solar cells (PVSCs) efficiency of 18.4%. Also, we incorporate the above-mentioned SAM into flexible PVSCs and achieved one of the highest PCE of 16.2% on PET substrate with a remarkable power-per-weight of 26.9 W/g

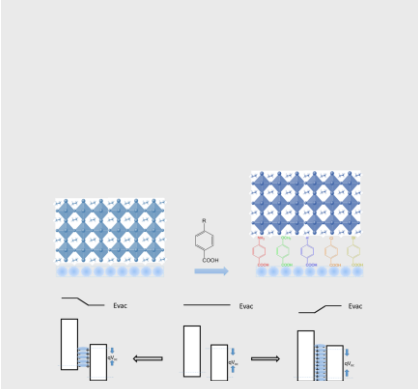

*Qin Wang[a,c], Chu-Chen Chueh[a], Ting Zhao[a], **Jiaqi Cheng**[d], Morteza Eslamian*[c], Wallace C.H. Choy[d] and Alex K.-Y. Jen*[a,b]*

Page No. – Page No.

Effects of Self-Assembling Monolayer Modification of NiO_x Nanoparticles Layer on the Performance of Inverted Perovskite Solar Cells and Its Application in High Power-Per-Weight Flexible Devices